Asian Journal of Chemistry; Vol. 38, No. 9 (2026), 2387-2397
ASIAN JOURNAL OF CHEMISTRY
https://doi.org/10.14233/ajchem.2026.36463

Silver Nanoparticles Augmented Polycystamine Coated Glassy Carbon Electrodes for Sensitive Sensing of *N*-Nitrosodimethylamine

RIDDHI TRIVEDI*, and PRAJESH PRAJAPATI

School of Pharmacy, National Forensic Sciences University, Gandhinagar-382007, India

*Corresponding author: E-mail: riddhitrivedi138@gmail.com

Received: 18 May 2026 *Accepted*: 6 August 2026 *Published online*: 5 September 2026 AJC-22466

Nitrosamine impurities, particularly *N*-nitrosodimethylamine (NDMA), are potent genotoxic and carcinogenic compounds that can pose significant risks even at trace concentrations. Their occurrence in pharmaceutical products, including cardiovascular, antidiabetic and gastro-retentive drugs, has raised major regulatory concerns, leading to recalls and restrictions on affected products. This study presents an electrochemical sensor for the trace-level detection of NDMA using a polymer-modified glassy carbon electrode (GCE). Silver nanoparticles embedded in polycystamine were integrated onto the GCE surface to enhance the analytical response, sensitivity and selectivity toward NDMA. The electrochemical behavior and quantitative detection of NDMA were investigated using cyclic voltammetry (CV), differential pulse voltammetry (DPV) and square-wave voltammetry (SWV). Surface morphology and modification of the electrode were examined by scanning electron microscopy (SEM). Interference studies were performed to assess the selectivity of the sensor in the presence of potentially coexisting species. The developed silver nanoparticle–polycystamine/GCE platform provides a sensitive and selective electrochemical approach for NDMA detection, with potential application in pharmaceutical quality control and analysis of complex industrial matrices.

Keywords: Nitroso compounds, Silver nanoparticle, Polycystamine, Electrochemical sensor, Voltammetric techniques.

INTRODUCTION

N-Nitrosodimethylamine (NDMA) is a highly toxic nitrosamine impurity associated with genotoxicity and carcinogenicity following prolonged exposure, even at low concentrations [1-3]. Its occurrence in pharmaceutical products has received considerable attention, particularly following the detection of NDMA in several drug classes, such as antihypertensive, antidiabetic and gastro-retentive medications [4-7]. Several sources of NDMA include pharmaceutical manufacturing effluents, wastewater, agricultural runoff and other industrial processes, creating potential pathways for its persistence and transport in aquatic systems [4-7]. Regulatory investigations initiated after the identification of nitrosamine contamination in pharmaceutical products led to recalls, manufacturing controls and the establishment of stringent limits for NDMA and related impurities [8,9]. Notable cases include the withdrawal of valsartan-containing products in 2018 and subsequent recalls and investigations involving ranitidine and metformin [10-13]. These events have established the need for reliable analytical methods capable of detecting NDMA at trace concentrations in pharmaceutical and environmental matrices [14-16].

Electrochemical sensing offers an attractive approach for NDMA determination owing to its potential for rapid analysis, low sample consumption, relatively simple instrumentation and compatibility with portable devices. Glassy carbon electrodes (GCEs) provide a stable and conductive platform for surface modification and electrochemical detection [17-21]. In the present work, polycystamine (poly-CA) was electropolymerized onto the GCE surface to construct a functional polymeric interface with accessible thiol groups and an enhanced the electroactive surface [22-25]. Silver nanoparticles (AgNPs) were incorporated into the polymer matrix to increase the electroactive area and facilitate interfacial electron transfer. The resulting AgNP/poly-CA/GCE architecture was investigated for NDMA detection using cyclic voltammetry (CV), differential pulse voltammetry (DPV) and square-wave voltammetry (SWV). Interference studies were performed to evaluate the selectivity of the sensor in the presence of potentially coexisting species relevant to complex samples [26,27].

A further feature of the proposed electrode is the green synthesis of AgNPs using *Hyphaene thebaica* extract, which provides a plant-mediated route that avoids conventional chemical reducing agents [28-32]. The integration of biosynthesized AgNPs with an electropolymerized poly-CA film provides a composite interface in which the thiol-containing polymer can facilitate nanoparticle immobilization, while the AgNP component contributes to the electrochemical response through its high surface activity and electron-transfer properties [33-36]. The sensor architecture is non-molecularly imprinted and does not require template incorporation or template removal procedures, offering a comparatively straightforward route to electrode fabrication.

Several electrochemical sensors based on molecularly imprinted polymers (MIPs) have been reported for NDMA determination. A MIP/polypyrrole/GCE sensor provided a linear range of 10-230 μg L^{-1} with a detection limit of 0.85 μg L^{-1} [37-39]. A dual-monomer MIP sensor based on linear sweep voltammetry achieved an LOD of 1.16 μg L^{-1} and permitted electrochemical regeneration [40,41]. A green synthesized AgNPs/chitosan/3-aminophenylboronic acid MIP sensor was reported to achieve an LOD of 3.63 fM using DPV [40,42]. A DNA/chitosan-carbon dot-based biosensor provided an LOD of 9.9 nM by DPV [43-45]. These reports establish MIPs and biomolecular recognition systems as effective strategies for achieving high analytical sensitivity, while their fabrication may involve additional recognition, template removal and surface-processing steps [41,46].

The present study explores a non-MIP AgNP/poly-CA/GCE platform for NDMA determination, with emphasis on a relatively simple electrode architecture, plant-mediated nanoparticle synthesis and electrochemical characterization. The objective was to evaluate the analytical response, sensitivity, selectivity and interference tolerance of the modified electrode toward trace NDMA and to assess its suitability for analysis in complex aqueous and pharmaceutical-related matrices. The proposed strategy is intended as a simpler alternative to recognition-layer-based sensors rather than as a direct replacement for MIP systems in terms of detection limit.

EXPERIMENTAL

Green synthesis of silver nanoparticles using *Hyphaene thebaica*: Silver nanoparticles (AgNPs) were synthesized using an aqueous extract of *H. thebaica* as a plant-mediated reducing and stabilizing agent. Briefly, 20 mL of the plant extract was added to 60 mL of 2 mM $AgNO_3$ solution under the specified reaction conditions. The reaction was visually monitored by the gradual change in colour from light brown to dark brown, which was attributed to the formation of AgNPs through the reduction of Ag^+ ions by phytochemicals present in the plant extract. The resulting suspension was centrifuged at 7000 rpm for 15 min to separate the nanoparticles from the reaction medium. The centrifugation and washing process was repeated three times to remove residual plant-derived components and unreacted silver ions. The resulting AgNPs precipitate was subjected to lyophilization to obtain a dry nanoparticle powder for subsequent characterization and electrode modification.

Fabrication of AgNPs/Poly-CA/modified GCE: The glassy carbon electrode (GCE) was mechanically polished with alumina slurry to obtain a smooth, mirror-like surface. The electrode was thoroughly rinsed with deionized water to remove residual alumina particles, followed by sonication in a 1:1 (v/v) methanol-nitric acid mixture to remove surface contaminants. The electrode was subsequently rinsed with acetone and distilled water and dried at room temperature.

Polycystamine (poly-CA) was electropolymerized on the cleaned GCE surface using a three-electrode configuration consisting of the GCE as the working electrode, a platinum wire as the counter electrode, and Ag/AgCl as the reference electrode. The polymerization solution contained 1 mM cystamine hydrochloride in 0.1 M phosphate-buffered saline (PBS). Electropolymerization was performed by cyclic voltammetry over a potential window of -1.3 to +2.6 V for 20 consecutive cycles. The resulting poly-CA coated electrode was rinsed thoroughly with distilled water and dried at room temperature.

The pre-synthesized silver nanoparticles (AgNPs), prepared were deposited onto the poly-CA/GCE surface by drop casting. The modified electrode was dried at room temperature under mild heating to promote adhesion of the nanoparticle layer. The resulting AgNPs/poly-CA/GCE was characterized by scanning electron microscopy (SEM) to assess surface morphology and confirm electrode modification. The electrochemical characteristics of the bare and modified electrodes were evaluated by cyclic voltammetry (CV) and square-wave voltammetry (SWV).

Preparation of NDMA standard solution: A standardized solution of the nitroso compounds (NDMA) stock solution with the composition of 5000 μg/mL was obtained commercially from Merck Chemicals. A 5 mM working solution was prepared with the final dilution of 10 mL methanol of NDMA. Filtration process was done with the Whatman grade filter paper with the quality mesh of 41 to remove filtrates from the solution. Finally, the calibration standards were prepared as 1 mM, 2 mM, 3 mM, 4 mM, 5 mM and was utilized for the experimental measurements.

Formation of poly-CA film: The poly-CA was deposited onto the GCE surface by electropolymerization using a conventional three-electrode cell comprising the GCE as the working electrode, a platinum wire as the counter electrode, and an Ag/AgCl electrode as the reference electrode. The electropolymerization was performed in an electrolyte solution containing cystamine hydrochloride as the monomer. Upon application of the selected potential range, oxidative polymerization of cystamine occurred at the GCE surface, resulting in the formation of a poly-CA film. The electropolymerization conditions were optimized by varying the applied potential window, cystamine concentration and electrolyte composition to obtain a stable and electrochemically active polymer film. The optimized poly-CA/GCE was subsequently used as the substrate for AgNPs deposition to construct the AgNPs/poly-CA/ GCE sensing interface.

Electrodeposition of poly-CA onto the GCE: The GCE with the clean surface was ready for the electrodeposition, the 1 mM cystamine hydrochloride solution was submerged and prepared in 0.1/m phosphate buffer saline. A 20 consecutive cycles of cyclic voltammetry was performed over the potential

window of -1.3 V to +2.6 V resulting into electro-oxidative polymerization of the cystamine on the surface of the electrode probe. The modified probe is thoroughly rinsed with the distilled water and dried at the room temperature. The formation of the thin film of poly-CA resulting in blue coloured film on GCE confirms and validates the successful electrodeposition.

Modification of poly-CA/GCE with AgNPs: The poly CA film is enhanced by deposition of AgNPs on the electrode probe. The pre-synthesized AgNPs suspension was deposited onto the poly-CA coated GCE surface by drop-casting to form the AgNPs/poly-CA/GCE composite electrode. Spin coating was subsequently employed as an alternative deposition method. The modified electrode was dried at room temperature under mild heating to stabilize the nanocomposite layer.

Electrochemical setup

Cyclic voltammetry (CV): Initial cyclic voltammetric measurements were performed using a bare glassy carbon electrode (GCE) over a potential range of -0.3 to -0.9 V at a constant scan rate of 0.1 V s^{-1}. A single irreversible reduction peak was observed for NDMA during the initial forward scan. The absence of a corresponding anodic peak during the reverse scan confirms the electrochemical irreversibility of the NDMA reduction process at the GCE surface.

Square wave voltammetry (SWV): SWV measurements were performed over a potential range of -0.3 to -0.9 V for the bare GCE, poly-CA/GCE and AgNPs/poly-CA/GCE electrodes under identical experimental conditions. The bare GCE exhibited a reduction peak at approximately -0.65 V, with a peak current of about 9 μA. The observed peak profile was associated with the electron-transfer process and adsorption of NDMA at the electrode surface.

LC-MS analysis of AgNPs and AgNPs/poly-CA/GCE: The developed LC–MS/MS method yielded a well-resolved NDMA peak at a retention time of approximately 2 min in the standard solution chromatogram and satisfied the established system suitability criteria.

Particle size analysis of AgNPs and AgNP/poly-CA/GCE/NDMA: Dynamic light scattering (DLS) and zeta potential measurements were performed to determine the hydrodynamic particle size distribution and colloidal stability of the green synthesized AgNPs and the AgNPs/poly-CA/GCE sensor after interaction with NDMA.

RESULTS AND DISCUSSION

UV-Vis studies: UV-Vis analysis of synthesized AgNPs at three different temperatures gave absorption maxima at 409, 407 and 404 nm, with corresponding absorbance values of 2.46047, 1.74153 and 1.29258, respectively. The absorbance decreased with increasing synthesis temperature across the investigated AgNPs concentration range of 10-30 ppb. Incorporation of poly-CA into the AgNPs/poly-CA/GCE system resulted in a further decrease in absorbance, as observed in the corresponding spectral response and UV standard curves (Fig. 1), which confirmed the interaction between the AgNPs and poly-CA matrix.

FTIR analysis: ATR-FTIR analysis was performed to examine the functional groups of NDMA and the interaction of NDMA with the AgNPs/poly-CA/GCE interface. Free NDMA exhibited characteristic absorption bands at approximately 2950, 1490 and 1365 cm^{-1}, which were assigned to C–H and N–N=O related vibrational modes. Following interaction with the AgNPs/poly-CA/GCE surface, these bands shifted to approximately 3293, 2981 and 1650 cm^{-1}, respectively (Fig. 2). The observed shifts are consistent with changes in the vibrational environment of NDMA upon interaction with the modified electrode surface and support the binding of NDMA to the poly-CA functionalized AgNP interface.

XRD analysis of AgNPs and AgNPs/poly-CA/GCE/NDMA: The crystalline structure of the synthesized AgNPs and AgNPs/poly-CA/GCE composite was investigated by X-ray diffraction (XRD). The XRD measurements were performed using Cu*K*α radiation (λ = 1.5406 Å) at 40 kV and 30 mA over a 2θ range of 20-80º. The XRD pattern of the AgNPs exhibited distinct diffraction peaks at approximately 38.1º, 44.3º, 64.4º and 77.5º in 2θ, which were assigned to the (111), (200), (220) and (311) crystallographic planes of face-centered cubic (FCC) metallic silver, respectively (Fig. 3).

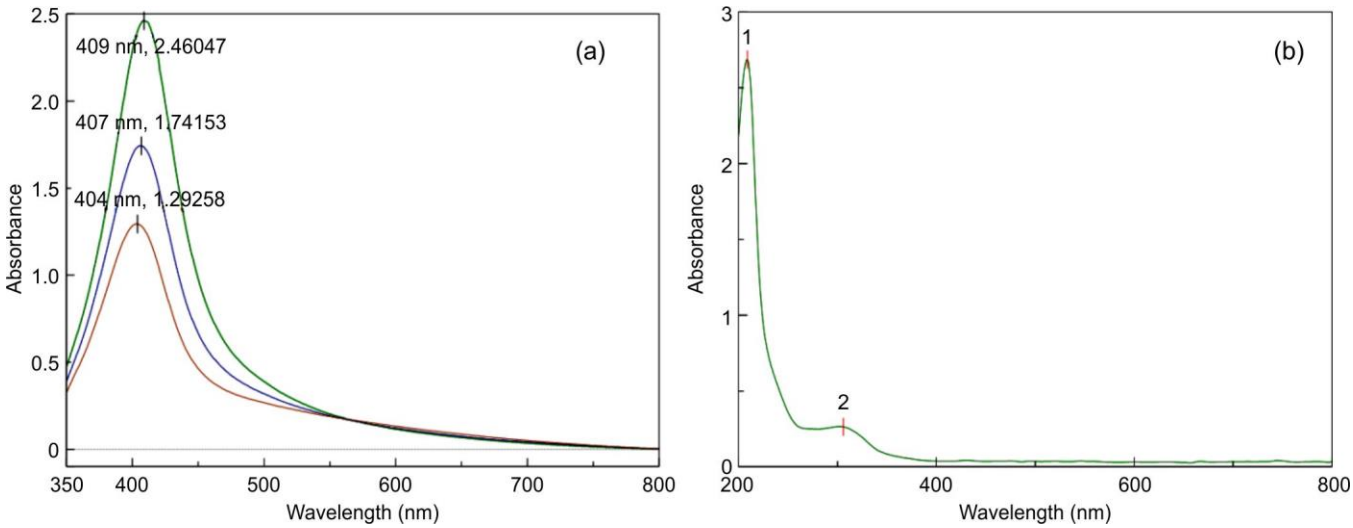

Fig. 1. UV spectra of the AgNPs (a) and AgNPs/poly-CA/GCE/NDMA (b)

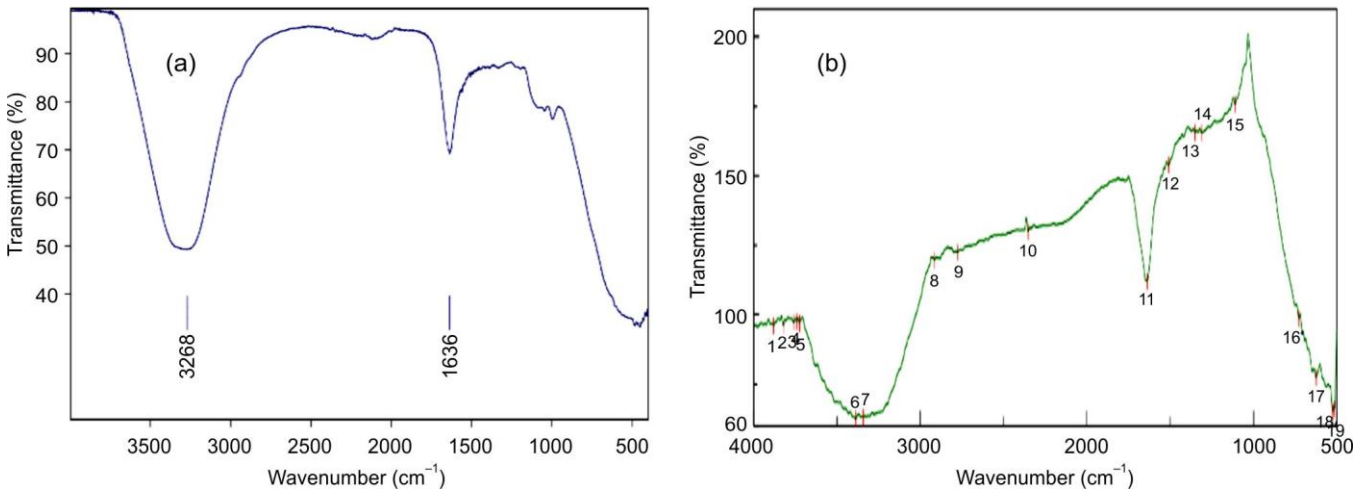

Fig. 2. FTIR spectra of the AgNPs (a) and AgNPs/poly-CA/GCE/NDMA (b)

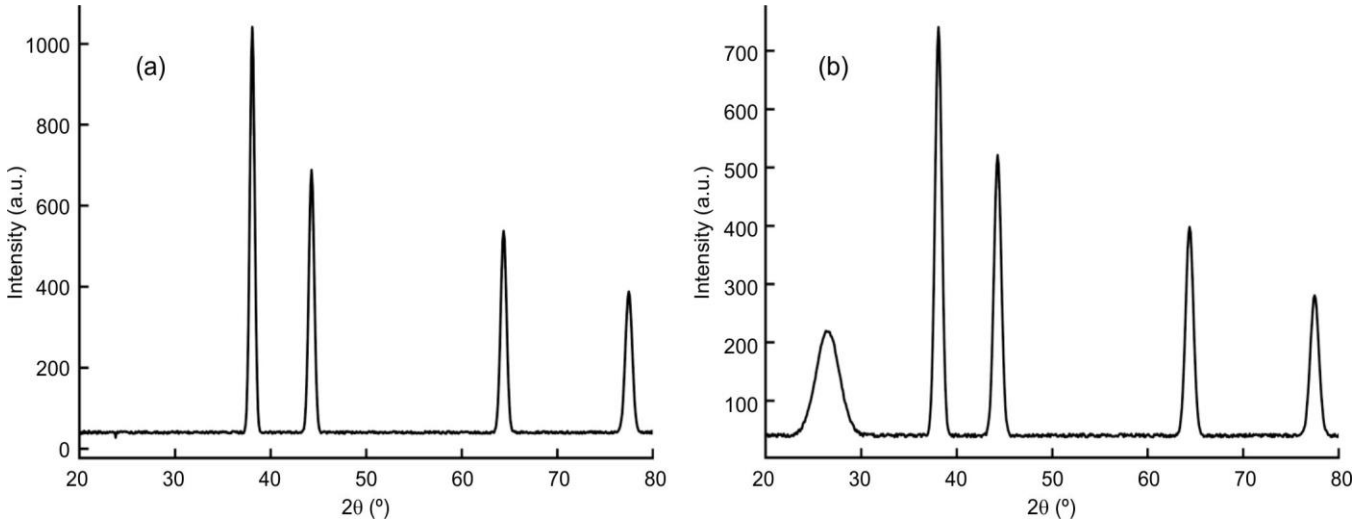

Fig. 3. XRD spectra of the AgNPs (a) and AgNPs/poly-CA/GCE/NDMA (b)

After immobilization onto the poly-CA/GCE surface, the characteristic Ag reflections were retained in the AgNPs/poly-CA/GCE pattern, confirming preservation of the Ag crystalline phase following electrode modification (Fig. 3a). Compared with the isolated AgNPs, the modified electrode exhibited lower diffraction intensity and broader Ag reflections, which can be associated with the lower relative amount and dispersion of AgNPs within the polymer-modified electrode matrix and the contribution of the polymer/substrate background. A broad feature in the lower-angle region was associated with the pre-dominantly amorphous nature of the poly-CA film. The retention of the characteristic Ag reflections after incorporation into the poly-CA/GCE interface supports the successful immobilization of crystalline AgNPs within the modified electrode architecture.

SEM studies: The SEM images reveal a progressive modification of the GCE surface following incorporation of the polymer matrix and silver nanoparticles. The bare GCE exhibits a relatively smooth and compact surface with limited morphological irregularity, consistent with its low surface roughness and absence of discernible particulate features. After modification with poly-CA, the electrode surface becomes distinctly rough and fibrous, forming an interconnected porous network (Fig. 4). As observed, there are larger accessible surface area and additional sites for electrochemical interactions compared with the bare GCE. Further incorporation of AgNPs results in a more heterogeneous and highly textured surface, with bright particulate features distributed within the polymer matrix. The embedded nanoparticles increase the density of electroactive sites and can facilitate electron-transfer processes at the electrode/electrolyte interface (Fig. 4).

The morphological changes are consistent with the electrochemical parameters. The electroactive area increases from 0.0862 cm^2 for the bare GCE to 0.1653 cm^2 for poly-CA/GCE confirmed that formation of the rough and porous polymer network substantially increases the accessible electrode surface. The AgNPs-modified electrode exhibits a markedly higher SWV peak current of 28.2567 μA, compared with 9.0234 μA for the bare GCE, further confirmed improved electrochemical response after nanoparticle incorporation. The rough porous architecture of the AgNPs/poly-CA composite, together with the high conductivity and large interfacial area associated with AgNPs, provides favourable conditions for electron transfer and analyte interaction. The shift in peak potential from ~0.65

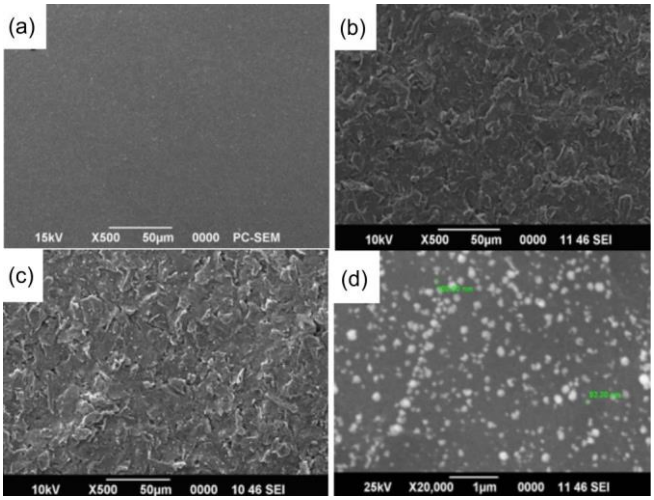

Fig. 4. SEM images of (a) bare GCE electrode, (b) poly-CA, (c) AgNPs/poly-CA/GCE and (d) AgNPs/poly-CA/GCE/NDMA

V for the bare GCE to -0.576 V for the AgNPs/poly-CA-modified electrode further indicates a substantial change in the interfacial electrochemical surface modification (Table-1).

Surface area analysis of poly-CA/GCE: The electroactive surface area of the bare GCE was estimated using a suitable redox probe and calculated as 0.0862 cm^2. Following electropolymerization of poly-CA, the electroactive surface area increased to 0.1653 cm^2. This increase may arise from the formation of a rougher and more electrochemically accessible polymer-modified interface (Fig. 5), providing a larger electrode-electrolyte contact area for electron-transfer processes.

Particle size analysis of AgNPs and AgNPs/poly-CA/GCE/NDMA: Dynamic light scattering (DLS) analysis gave an average hydrodynamic diameter of approximately 57 nm for the synthesized AgNPs, with a polydispersity index (PDI) of approximately 0.50. After functionalization with the poly-CA/GCE interface and subsequent interaction with NDMA, the measured hydrodynamic diameter increased to ~418.3 nm, while the PDI decreased to 0.262 (Fig. 6). The increase in hydrodynamic size may be associated with surface functionalization and the formation of larger associated structures involving AgNPs and the poly-CA matrix. The lower PDI after functionalization suggests a narrower particle-size distribution relative to the initial AgNPs dispersion. The DLS results support the formation of the AgNPs/poly-CA-based sensing interface and its subsequent interaction with NDMA.

SWV behaviour of NDMA at bare GCE, poly-CA/GCE and AgNPs/poly-CA/GCE: Square-wave voltammetry (SWV) was used to evaluate and compare the electrochemical response of NDMA at bare GCE, poly-CA/GCE and AgNPs/poly-CA/GCE. At an NDMA concentration of 10 ng, the bare GCE exhibited a cathodic reduction peak with a current of 9.0234 µA within the investigated potential range (Table-2). The relatively weak and poorly defined response at the bare GCE is consistent with limited electron-transfer kinetics at the

TABLE-1
COMPARATIVE SEM AND ELECTROCHEMICAL CHARACTERISTICS OF BARE GCE, Poly-CA/GCE AND AgNPs/Poly-CA/GCE

Electrode stage	Surface texture	Porosity	Roughness	Particle presence	Electroactive area (cm^2)	SWV peak current (µA)	Peak potential (V)
Bare GCE	Smooth/flat	None	Low	None	0.0862	9.0234	~ -0.65
Poly-CA/GCE	Rough/fibrous network	High	High	None (polymer only)	0.1653	Enhanced (*vs.* bare)	Improved
AgNPs/Poly-CA/GCE	Rough & porous	High	High	AgNPs embedded in matrix	Not measured separately	28.2567	-0.576
Surface area % increase (Bare → Poly-CA)							

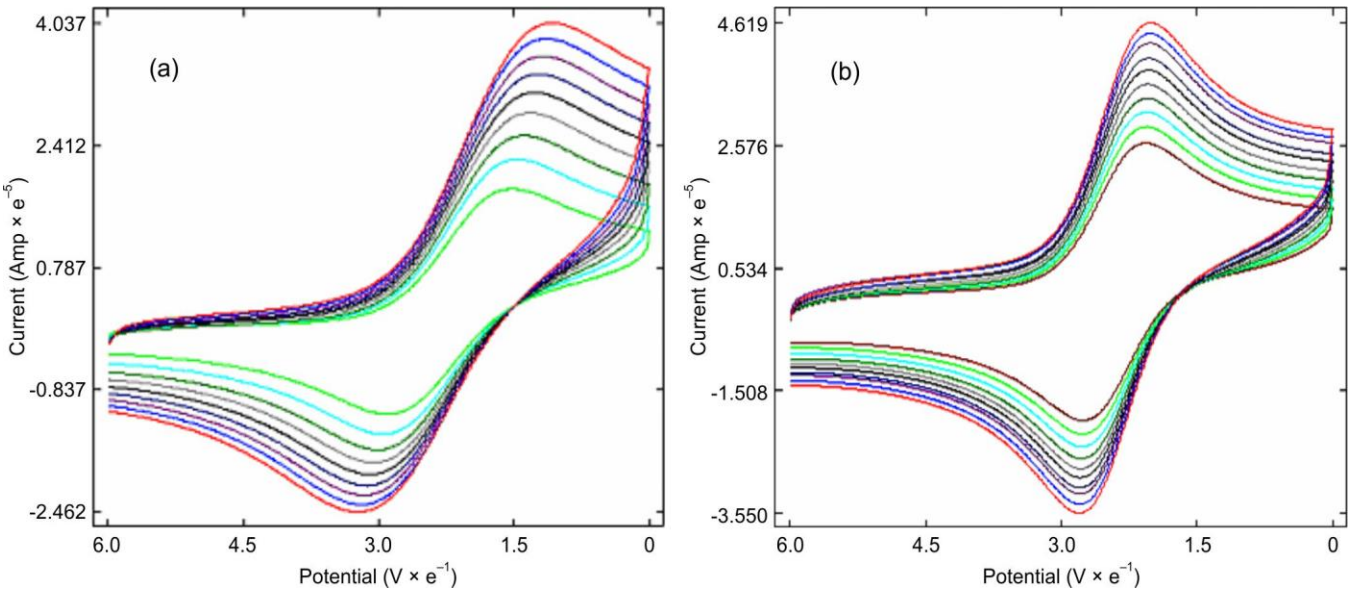

Fig. 5. Cyclic voltammograms of (a) bare GCE and (b) AgNPs/poly-CA/GCE towards NDMA

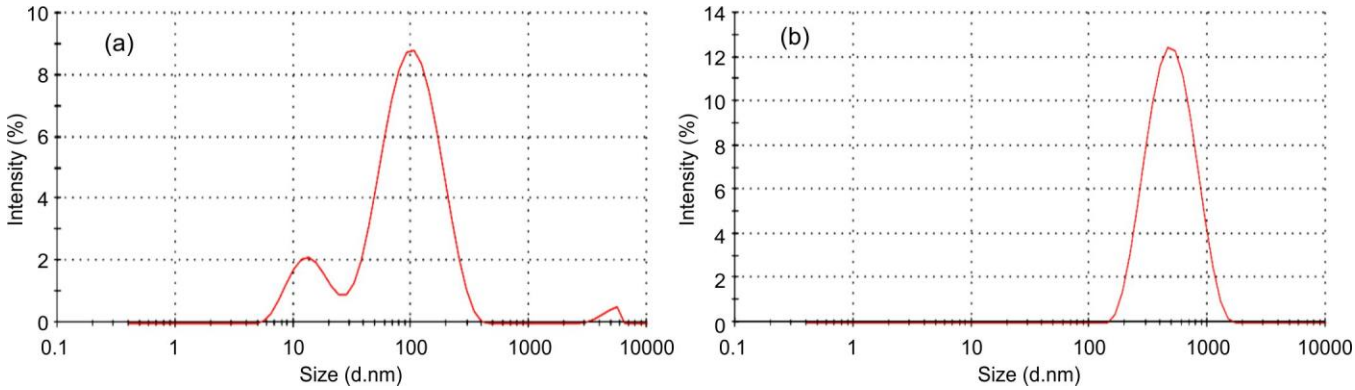

Fig. 6. Particle size analysis of AgNPs (a) and AgNPs/poly-CA/GCE/NDMA (b)

TABLE-2
COMPARATIVE CYCLIC VOLTAMMETRY AND SWVWAVE VOLTAMMETRY
PARAMETERS OF BARE AND MODIFIED GCE ELECTRODES

Electrode	Potential range (V)	Scan rate (V/s)	Peak potential (V)	Peak current (μA)
Bare GCE	-0.3 to -0.9	0.06	~ -0.65	9.0234
Poly-CA/GCE	-0.3 to -0.9	0.06	Improved	Enhanced
AgNPs/poly-CA/GCE	-0.2 to -0.8	0.06	-0.576	28.2567

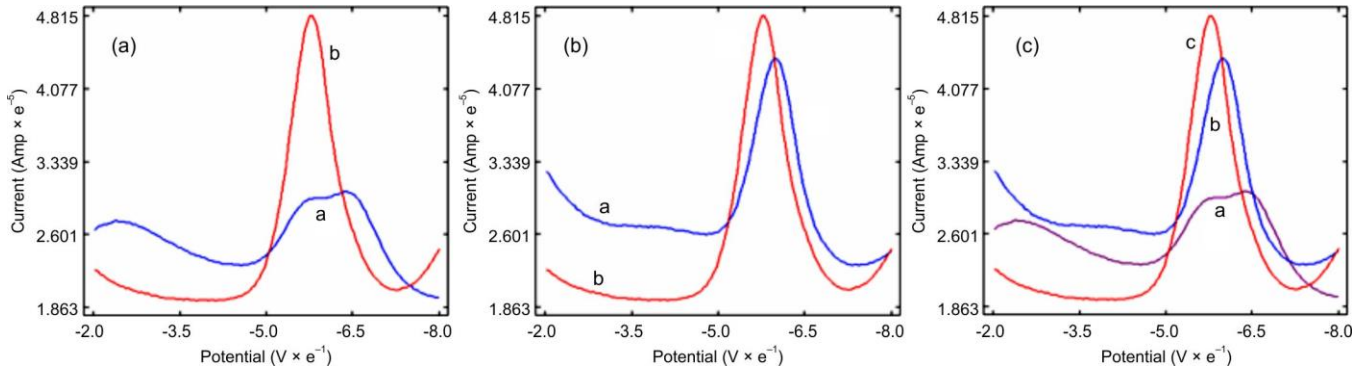

Fig. 7. Comparative SWV performances (a) bare GCE, (b) poly-CA/AgNPs and (c) AgNPs/poly-CA/GCE/NDMA

unmodified electrode surface. Modification with poly-CA increased the electrochemically accessible surface area and altered the interfacial electron-transfer characteristics, resulting in an enhanced NDMA response. The AgNPs/poly-CA/GCE exhibited the strongest electrochemical response, with a sharp cathodic peak at -0.576 V and a peak current of 28.2567 μA when measured at a scan rate of 0.06 V s^{-1} over the potential range of -0.2 to -0.8 V (Fig. 7). The peak current was approximately three times higher than that obtained at the bare GCE, accompanied by a shift of approximately 70 mV in the peak potential. The enhanced response is associated with the increased electroactive surface area and improved interfacial electron transfer provided by the poly-CA/AgNPs composite interface, supporting the contribution of both electrode components to the electrochemical detection of NDMA.

CV response of AgNPs/poly-CA/GCE toward NDMA: The CV was used to compare the electrochemical response of the bare GCE and AgNPs/poly-CA/GCE toward NDMA. A single cathodic reduction peak was observed during the forward scan, while no corresponding anodic peak appeared during the reverse scan, consistent with an electrochemically irreversible reduction process (Fig. 8). The AgNPs/poly-CA/GCE exhibited a substantially enhanced reduction current

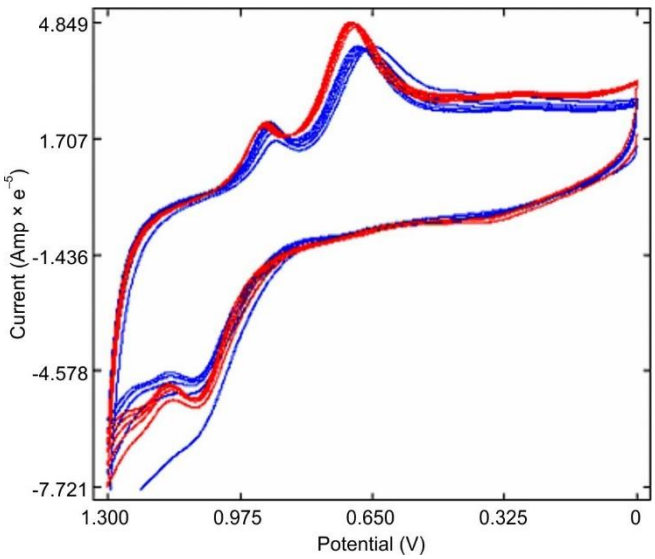

Fig. 8. CV graph of AgNPs/poly-CA/NDMA

compared with the bare GCE, which is attributed to the increased electroactive surface area and improved electron-transfer characteristics of the nanocomposite interface. The enhanced cathodic

response supports the application of AgNPs/poly-CA/GCE for electrochemical detection of NDMA (Table-3).

Effect of pH: The influence of the NDMA on different pH systems was analyzed with 0.1 M phosphate, acetate, citrate buffer with the salts such as sulphuric acid, sodium hydroxide, potassium nitrate and sodium chloride. Parameters including peak current, peak potential and shape were assessed to gain thermodynamics and influence of electrolyte medium on NDMA detection. The phosphate buffer medium was therefore selected for all subsequent electrochemical measurements (Fig. 9).

Effect of scan rate: The relation between scan rate and current peak was investigated between 30 and 170 mV s^{-1} for 10 ppb NDMA solution (Fig. 10). The current increased on the nanocomposite probe compare to the bare probe indicates the kinetics at the electrode enhanced due to mass transport on the surface of electrode. In the composite the electrocatalytic property amplification for AgNPs reinforcing better analytical performance.

Differential pulse voltammetry (DPV): Concentration study: Differential pulse voltammetry (DPV) was employed for the quantitative determination of NDMA using the bare GCE and AgNPs/poly-CA/GCE at 25 ºC. For the bare GCE, NDMA concentrations of 10, 30, 50 and 70 ppb and 1 ppm were investigated and the resulting calibration plot showed a linear response with a regression coefficient (R^2) of 0.98752 (Fig. 11). For the AgNPs/poly-CA/GCE, the concentration range was extended from 10 ppb to 10 ppm, with measurements performed at 10, 50, 70 and 90 ppb and 2, 6, 8 and 10 ppm. The concentration-dependent increase in peak current obtained with the modified electrode (Fig. 12) provided improved analytical sensitivity compared with the bare GCE, supporting the application of the AgNPs/poly-CA/GCE platform for trace-level NDMA determination.

LC-MS analysis: LC-MS analysis was performed to evaluate the NDMA response of the AgNPs/poly-CA/GCE sensing system. The chromatographic profiles of NDMA and

TABLE-3
COMPARATIVE DATA OF DPV CONCENTRATION RANGE FOR BARE GCE, POLY-CA/GCE AND AgNPS/POLY-CA/GCE

Bare GCE/poly-CA/GCE – Concentrations tested				
Conc. (ppb)	Conc. (ppm)	Approx. molarity (M)	Electrode	Inference
10	0.01	~1×10^{-5}	Bare GCE/poly-CA/GCE	
30	0.03	~3×10^{-5}	Bare GCE	
50	0.05	~5×10^{-5}	Bare GCE/poly-CA/GCE	
70	0.07	~7×10^{-5}	Bare GCE/poly-CA/GCE	
1000	1	~1×10^{-3}	Bare GCE	Upper limit
AgNPs/Poly-CA/GCE – Full concentration range (10 ppb–10 ppm)				
Conc. (ppb)	Conc. (ppm)	Series	Approx. molarity (M)	Inference
10	0.01	ppb range	~1×10^{-5}	
50	0.05	ppb range	~1×10^{-5}	
70	0.07	ppb range	~1×10^{-5}	
90	0.09	ppb range	~1×10^{-5}	
2000	2	ppm range	~1×10^{-5}	
6000	6	ppm range	~1×10^{-5}	
8000	8	ppm range	~1×10^{-5}	
10000	10	ppm range	~1×10^{-5}	Upper limit
Calibration R^2 = 0.98752 (linear); nanocomposite shows higher selectivity & sensitivity than bare GCE				

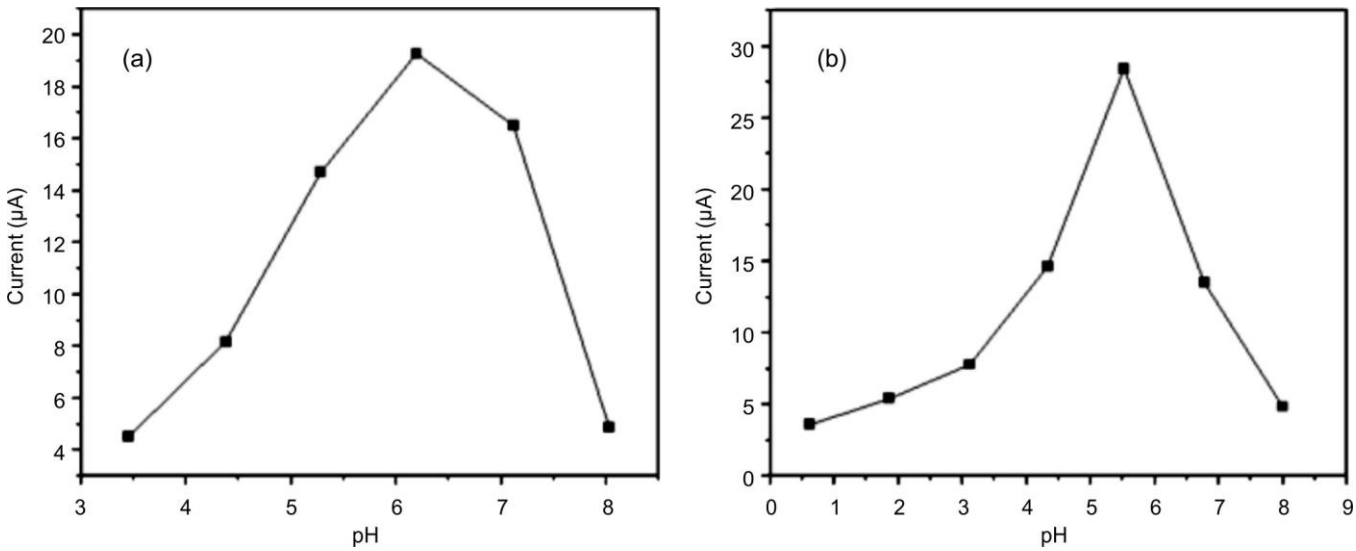

Fig. 9. Effect of pH on the DPV response of NDMA at (a) Poly-CA/GCE and (b) AgNPs/Poly-CA/GCE

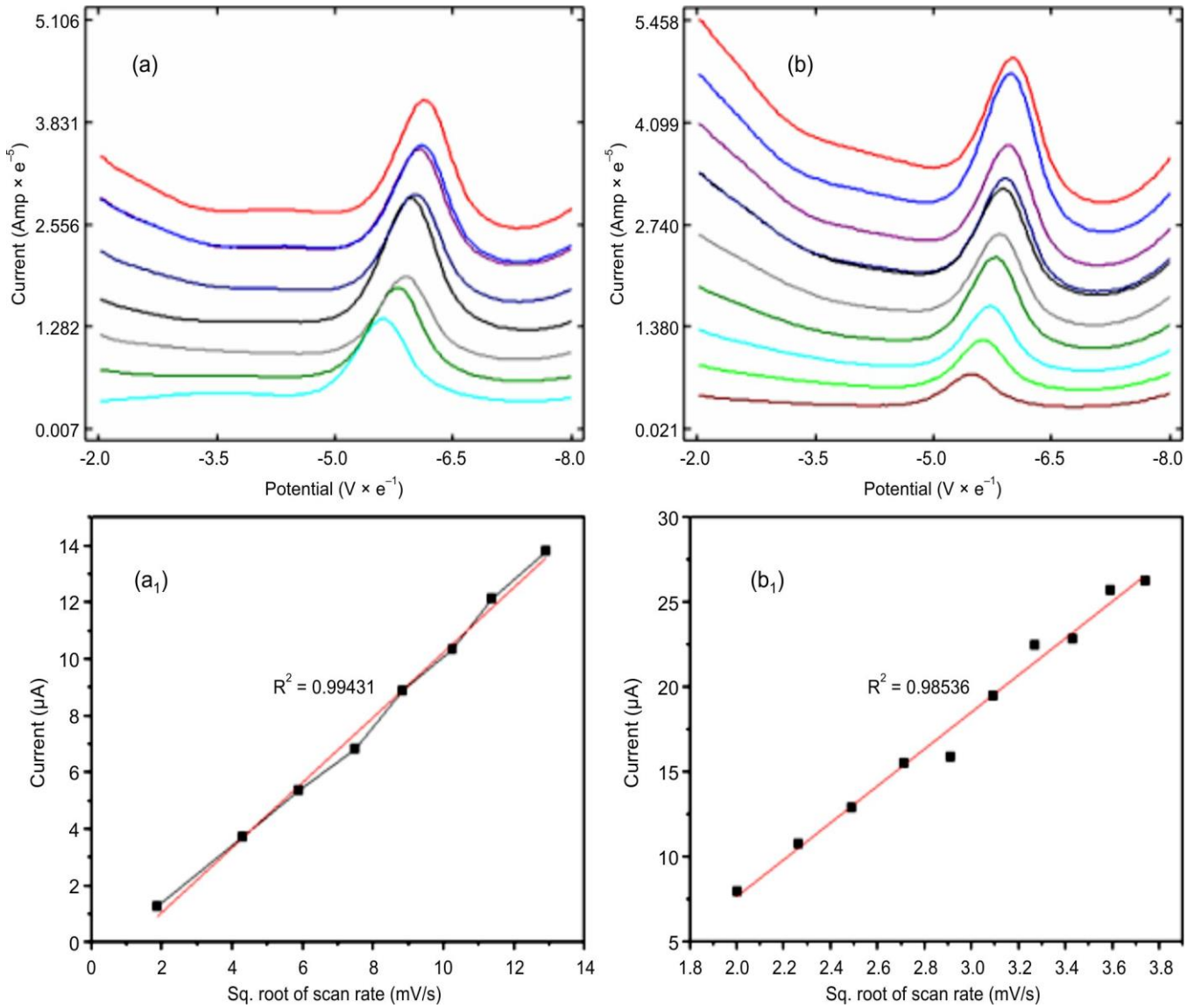

Fig. 10. Effect of scan rate on the DPV response of NDMA at (a, a_1); poly-CA/GCE and (b, b_1) AgNPs/poly-CA/GCE

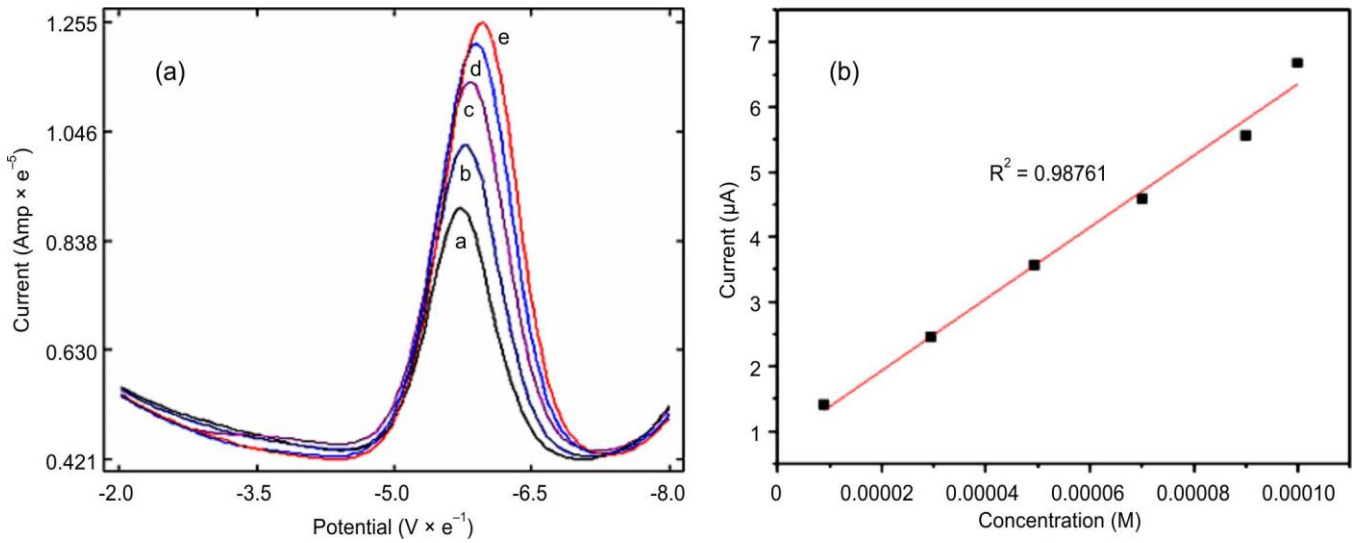

Fig. 11. DPV responses of AgNPs/poly-CA/GCE at different NDMA concentrations and the corresponding calibration plot

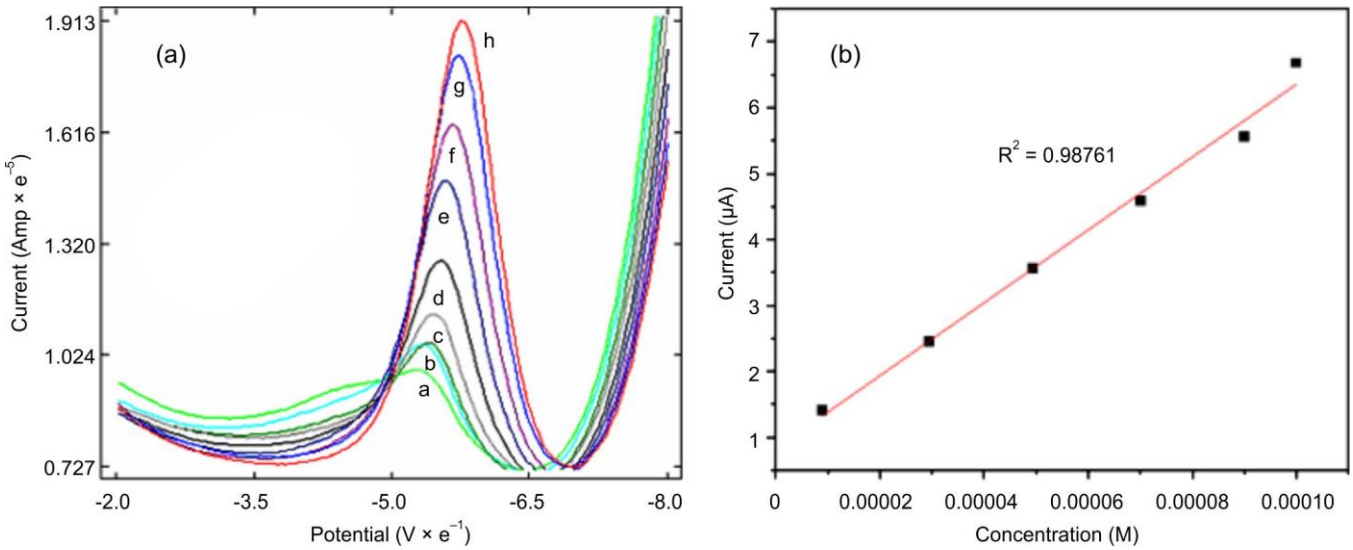

Fig. 12. Differential pulse voltammograms of NDMA of different concentrations (a) 10 ppb, (b) 50 ppb, (c) 70 ppb, (d) 90 ppb, (e) 2 ppm, (f) 6 ppm, (g) 8 ppm, (h) 10 ppm at AgNPs/poly-CA/GCE at 25 ºC

the AgNPs/poly-CA/GCE/NDMA complex exhibited a retention time of approximately 6 min, with intensities of 9×10^4 for NDMA and 3.1×10^5 for the AgNPs/poly-CA/GCE/NDMA complex, respectively (Fig. 13). NDMA-bound nanoparticle samples with three different Z-average particle sizes (42, 55 and 79 nm) were analyzed and the corresponding parameters are summarized in Table-4.

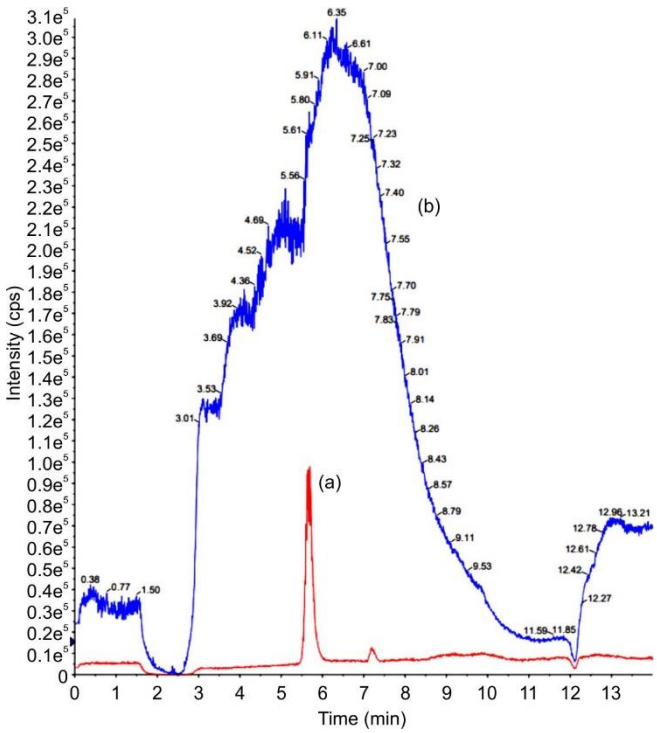

Fig. 13. LC-MS spectra of AgNPs (a) and AgNPs/poly-CA/GCE/NDMA (b)

Validation of LOD and LOQ: The analytical sensitivity of the developed LC-MS/MS method was assessed by determining the limit of detection (LOD) and limit of quantification (LOQ) for NDMA. The LOD and LOQ were calculated

TABLE-4
LC-MS/MS PEAK CHARACTERISTICS OF NDMA STANDARD AND NANOPARTICLE-BOUND SAMPLES WITH DIFFERENT PARTICLE SIZES

Sample	Analyte peak area (counts)	Analyte retention time (min)
100 ppb standard	1,900,044	5.347
Sample 1 (42 nm)	476,624	5.662
Sample 2 (55 nm)	723,662	5.622
Sample 3 (79 nm)	1,059,913	5.684

using the standard deviation of the response and the slope of the calibration curve, in accordance with ICH Q2(R1) guidelines. The obtained LOD and LOQ values were 63 and 164 ng mL^{-1}, respectively, supporting the applicability of the method for the detection and quantification of NDMA at trace concentrations in nanoparticle-bound samples (Table-5).

TABLE-5
ANALYTICAL PARAMETERS FOR THE DETERMINATION OF LOD AND LOQ OF NDMA BY LC-MS/MS

Parameters	NDMA
Mean of slope	17673
Standard deviation of intercepts	312
LOD	63
LOQ	164

Repeatability and intermediate precision: Repeatability was assessed using at least six replicate injections of the same NDMA standard concentration under identical conditions on the same day, using the same instrument and analyst. The mean, standard deviation (SD) and relative standard deviation (%RSD) were calculated for the peak area and retention time. Intermediate precision was assessed by repeating the replicate measurements on different days and, where applicable, using a different analyst or instrument to evaluate the consistency of the method under varying analytical conditions. The %RSD values obtained from the intra-day and inter-day

TABLE-6
INTRA-DAY AND INTER-DAY PRECISION OF THE LC-MS/MS METHOD FOR NDMA DETERMINATION

Drug	Concentration (ng/mL)	Intra-day		Inter-day	
		Mean ± SD	CV	Mean ± SD	CV
NDMA	4	4359780 ± 4412	0.27	4178678 ± 462	1.92
	6	6051440 ± 6035	0.16	6512446 ± 5675	1.84
	8	7487442 ± 8553	0.10	7123876 ± 7665	1.56

TABLE-7
EFFECT OF COMMON CO-EXISTING SPECIES ON THE RESPONSE OF THE AgNPS/POLY-CA/GCE SENSOR TOWARD NDMA

Substance	Concentration (ppm)	Current (μA)	Signal change (%)	Accepted (≤ 5%)	Category
NDMA	10	18.7425	–	N/A	Analyte
Urea	1000	17.9832	4.05	Yes	Biological
Sodium	1000	19.2154	2.52	Yes	Ion
Potassium	1000	18.0216	3.85	Yes	Ion
Glucose	1000	19.0837	1.82	Yes	Biological
Chloride	1000	19.3542	3.27	Yes	Ion
Ascorbic acid	1000	18.2648	2.55	Yes	Biological
Sulfate	1000	18.1023	3.41	Yes	Chemical
Lactose	1000	19.4821	3.94	Yes	Excipient

measurements were used to assess the precision of the LC-MS/MS method, with %RSD values of ≤ 2% considered indicative of good precision for the analytical procedure (Table-6).

Interference study: The selectivity of the AgNPs/poly-CA/GCE sensor toward NDMA was evaluated in the presence of potentially interfering physiological, pharmaceutical and environmental constituents. The selected interferents were tested at 1000 ppm, corresponding to a 100-fold excess relative to the NDMA analyte concentration of 10 ppm. The investigated species included urea, Na^+, K^+, glucose, Cl^-, ascorbic acid and lactose. The response obtained for NDMA remained within 5% of the baseline response in the presence of these potentially interfering species, supporting the selectivity of the modified electrode for NDMA determination. The results of the interference study are summarized in Table-7.

Conclusion

The AgNPs/poly-CA/GCE platform was developed for electrochemical determination of *N*-nitrosodimethylamine (NDMA) in pharmaceutical and aqueous matrices. Electropolymerization of cystamine increased the electroactive surface area of the GCE from 0.0862 to 0.1653 cm^2, while incorporation of AgNPs enhanced interfacial electron transfer. SWV yielded a well-defined cathodic peak at -0.576 V with a peak current of 28.2567 mA, compared with 9.0234 mA for the bare GCE. The CV measurements confirmed an electrochemically irreversible reduction process, with no corresponding anodic peak during the reverse scan. UV-Vis, ATR-FTIR, XRD and DLS characterization supported the formation of the AgNPs/poly-CA interface and its interaction with NDMA. pH and scan-rate studies, followed by DPV measurements, established the electrochemical response of the modified electrode across the investigated concentration range. The selectivity study used urea, Na^+, K^+, glucose, Cl^-, ascorbic acid and lactose at a 100-fold excess relative to NDMA, with signal deviations within 5%. LC-MS/MS analysis provided independent confirmation of NDMA detection, with LOD and LOQ values of 63 and 164 ng mL^{-1}, respectively. The combination of electropolymerized poly-CA and green synthesized AgNPs provides a simple non-MIP sensing architecture that avoids template-removal procedures. The AgNPs/poly-CA/GCE electrode has potential for rapid NDMA screening in pharmaceutical and water samples, with further validation in real matrices required to establish its practical analytical applicability.

CONFLICT OF INTEREST

The authors declare that there is no conflict of interests regarding the publication of this article.

DECLARATION OF AI-ASSISTED TECHNOLOGIES

During the preparation of this manuscript, the authors used an AI-assisted tool(s) to improve the language and no data, results or scientific conclusions were generated by AI. All analyses, interpretations and conclusions are the authors' own. The authors reviewed and edited the content and take full responsibility for the published work.

REFERENCES

1. D. Singh, S. Jain, T. Kaur and D. Rawat, *Crit. Rev. Anal. Chem.*, (2026); https://doi.org/10.1080/10408347.2025.2612233
2. Z. Guo, H. Feng and T.M. Swager, *ACS Sens.*, **10**, 881 (2025); https://doi.org/10.1021/acssensors.4c02462
3. M. Fritzsche, G. Blom, J. Keitel, A. Goettsche, M. Seegel, S. Leicht, B. Guessregen, S. Hickert, P. Reifenberg, A. Cimelli, R. Baranowski, E. Desmartin, E. Barrau, M. Harrison, T. Bristow, N. O'Neill, A. Kirsch, P. Krueger, C. Saal, B. Mouton and J. Schlingemann, *Eur. J. Pharm. Sci.*, **168**, 106026 (2022); https://doi.org/10.1016/j.ejps.2021.106026
4. Y.D. Liu, M. Selbes, C. Zeng, R. Zhong and T. Karanfil, *Environ. Sci. Technol.*, **48**, 8653 (2014); https://doi.org/10.1021/es500997e
5. S. Shukla and S. Behere, *Asian J. Res. Pharm. Sci.*, **14**, 373 (2024); https://doi.org/10.52711/2231-5659.2024.00059
6. S. Schmidtsdorff, J. Neumann, A.H. Schmidt and M.K. Parr, *Arch. Pharm.*, **355**, 2100435 (2022); https://doi.org/10.1002/ardp.202100435

7. B.L. Kasinath and B. Veeraswami, *Res. J. Pharm. Technol.*, **18**, 5041 (2025); https://doi.org/10.52711/0974-360X.2025.00728
8. S. Milmo, *Pharm. Technol.*, **44**, 6 (2020); https://doi.org/10.55126/ijzab.2025.v10.i06.SP074
9. H.P.R. Vikram, T.P. Kumar, G. Kumar, N.M. Beeraka, R. Deka, S.M. Suhail, S. Jat, N. Bannimath, G. Padmanabhan, R.S. Chandan, P. Kumar and B. Gurupadayya, *J. Pharm. Anal.*, **14**, 100919 (2024); https://doi.org/10.1016/j.jpha.2023.12.009
10. M.T. Farcas, E.R. Kisin, A. Menas, D.W. Gutkin, A. Star, R. Reiner, N. Yanamala, K. Savolainen and A.A. Shvedova, *J. Toxicol. Environ. Health A*, **79**, 984 (2016); https://doi.org/10.1080/15287394.2016.1211045
11. P. Couvreur and F. Puisieux, *Adv. Drug Deliv. Rev.*, **10**, 141 (1993); https://doi.org/10.1016/0169-409X(93)90046-7
12. D. Świeczkowski, S. Zdanowski, P. Merks, Ł. Szarpak, R. Vaillancourt and M.J. Jaguszewski, *Cardiol. J.*, **29**, 133 (2022); https://doi.org/10.5603/CJ.a2020.0168
13. J.A. Wagner, J. Dinh, J.R. Lightdale, B.D. Gold and J.M. Colombo, *Clin. Transl. Sci.*, **14**, 1197 (2021); https://doi.org/10.1111/cts.12995
14. R. Řemínek, F. Foret and D.S. Chung, *Electrophoresis*, **42**, 334 (2021); https://doi.org/10.1002/elps.202000303
15. H. Lim, Y. Oh and H. Shin, *J. Pharm. Biomed. Anal.*, **189**, 113460 (2020); https://doi.org/10.1016/j.jpba.2020.113460
16. M. Ghalkhani, N.K. Bakırhan and S.A. Özkan, *Crit. Rev. Anal. Chem.*, **50**, 538 (2020); https://doi.org/10.1080/10408347.2019.1664281
17. H. Karimi-Maleh, F. Karimi, M. Alizadeh and A.L. Sanati, *Chem. Rec.*, **20**, 682 (2020); https://doi.org/10.1002/tcr.201900092
18. A.M.R. Sylvia, C. Vedhi and A. Gomathi, *J. Nanosci. Technol.*, **4**, 567 (2018); https://doi.org/10.30799/jnst.181.18040528
19. A. Umar, M.M. Rahman and Y. Hahn, *J. Nanosci. Nanotechnol.*, **9**, 4686 (2009); https://doi.org/10.1166/jnn.2009.1103
20. C.A. Otuechere, A. Adewuyi, T. Oluwabayo, F. Afolayan, O.J. Avwioroko and U. Abazuh, *Andrologia*, **52**, e13426 (2019); https://doi.org/10.1111/and.13426
21. J.G. Manjunatha, *Open Chem. Eng. J.*, **13**, 81 (2019); https://doi.org/10.2174/1874123101913010081
22. J. Scremin, G.J. Mattos, R.D. Crapnell, S.J. Rowley-Neale, C.E. Banks and E.R. Sartori, *Electroanalysis*, **33**, 526 (2021); https://doi.org/10.1002/elan.202060172
23. M. Vomero, E. Castagnola, F. Ciarpella, E. Maggiolini, E. Zucchini, N. Goshi, S. Carli, L. Fadiga, S. Kassegne and D. Ricci, *Sci. Rep.*, **7**, 40332 (2017); https://doi.org/10.1038/srep40332
24. P.T. Lee and R.G. Compton, *Electroanalysis*, **25**, 1613 (2013); https://doi.org/10.1002/elan.201300145
25. M.M. Habibi, M. Mousavi, M. Shekofteh-Gohari, A. Parsaei-Khomami, M.-A. Hosseini, E. Haghani, R. Salahandish and J.B. Ghasemi, *Sci. Rep.*, **14**, 8099 (2024); https://doi.org/10.1038/s41598-024-58843-9
26. A.Z. Almenhali, P. Kanagavalli, M. Abd-Ellah, S. Khazaal, N. El Darra and S. Eissa, *Sci. Rep.*, **15**, 10329 (2025); https://doi.org/10.1038/s41598-025-94313-6
27. F. Khan, M. Shariq, M. Asif, M.A. Siddiqui, P. Malan and F. Ahmad, *Nanomaterials*, **12**, 673 (2022); https://doi.org/10.3390/nano12040673
28. N. Rana, A.N. Banu, B. Kumar, S.K. Singh, N.E. Abdel-razik, N.A. Jalal, F. Bantun, E. Vamanu and M.P. Singh, *Front. Microbiol.*, **15**, 1399937 (2024); https://doi.org/10.3389/fmicb.2024.1399937
29. S. Ahmad, S. Munir, N. Zeb, A. Ullah, B. Khan, J. Ali, M. Bilal, M. Omer, M. Alamzeb, S.M. Salman and S. Ali, *Int. J. Nanomedicine*, **14**, 5087 (2019); https://doi.org/10.2147/IJN.S200254
30. S. Jebril, A. Fdhila and C. Dridi, *Sci. Rep.*, **11**, 22060 (2021); https://doi.org/10.1038/s41598-021-01609-4
31. N. Liaqat, N. Jahan, Khalil-ur-Rahman, T. Anwar and H. Qureshi, *Front. Chem.*, **10**, 952006 (2022); https://doi.org/10.3389/fchem.2022.952006
32. V.-D. Doan, T.L. Phan, V.T. Le, Y. Vasseghian, L.O. Evgenievna, D.L. Tran and V.T. Le, *Chemosphere*, **286**, 131894 (2022); https://doi.org/10.1016/j.chemosphere.2021.131894
33. X. Gao, S. Dong, L. Fu, B. Zhang, H. Hsu and G. Zou, *Anal. Chem.*, **93**, 3295 (2021); https://doi.org/10.1021/acs.analchem.0c05342
34. B. Barton, N. Ullah, K. Koszelska, S. Smarzewska, W. Ciesielski and D. Guziejewski, *Environ. Sci. Pollut. Res. Int.*, **31**, 37923 (2024); https://doi.org/10.1007/s11356-024-33676-1
35. V. Ayerdurai, M. Cieplak and W. Kutner, *Trends Analyt. Chem.*, **158**, 116830 (2023); https://doi.org/10.1016/j.trac.2022.116830
36. B. Cui, P. Liu, X. Liu, S. Liu and Z. Zhang, *J. Mater. Res. Technol.*, **9**, 12568 (2020); https://doi.org/10.1016/j.jmrt.2020.08.052
37. L. Wang, M. Pagett and W. Zhang, *Sens. Actuators Rep.*, **5**, 100153 (2023); https://doi.org/10.1016/j.snr.2023.100153
38. J. Ashley, M.-A. Shahbazi, K. Kant, V.A. Chidambara, A. Wolff, D.D. Bang and Y. Sun, *Biosens. Bioelectron.*, **91**, 606 (2017); https://doi.org/10.1016/j.bios.2017.01.018
39. N.S. Shah, V. Thotathil, S.A. Zaidi, H. Sheikh, M. Mohamed, A. Qureshi and K.K. Sadasivuni, *Biosensors*, **12**, 1107 (2022); https://doi.org/10.3390/bios12121107
40. M. Zahran, Z. Khalifa, M.A.-H. Zahran and M. Abdel Azzem, *Mater. Adv.*, **2**, 7350 (2021); https://doi.org/10.1039/D1MA00769F
41. C. Bartolucci, A. Antonacci, F. Arduini, D. Moscone, L. Fraceto, E. Campos, R. Attaallah, A. Amine, C. Zanardi, L.M. Cubillana-Aguilera, J.M. Palacios Santander and V. Scognamiglio, *Trends Analyt. Chem.*, **125**, 115840 (2020); https://doi.org/10.1016/j.trac.2020.115840
42. A.C. Anbalagan, J. Korram, M. Doble and S.N. Sawant, *Discov. Nano*, **19**, 37 (2024); https://doi.org/10.1186/s11671-024-03980-3
43. S. Hassani, M. Rezaei Akmal, A. Salek Maghsoudi, S. Rahmani, F. Vakhshiteh, P. Norouzi, M.R. Ganjali and M. Abdollahi, *Front. Bioeng. Biotechnol.*, **8**, 574846 (2020); https://doi.org/10.3389/fbioe.2020.574846
44. D.J. Denmark, S. Mohapatra and S.S. Mohapatra, *EuroBiotech. J.*, **4**, 184 (2020); https://doi.org/10.2478/ebtj-2020-0023
45. T. Lazarević-Pašti, T. Tasić, V. Milanković and N. Potkonjak, *Chemosensors*, **11**, 35 (2023); https://doi.org/10.3390/chemosensors11010035
46. E.-S. Choi, J.-H. Kim, Y. Na, B.G. Lee, M. Yeo and E. Kim, *Sci. Rep.*, **16**, 16880 (2026); https://doi.org/10.1038/s41598-026-47624-1